Heterogeneous nuclei effect of MgAl2O4 on NbC in Fe matrix MMC coating

Zhao Changchun[a], Zhou Yefei[a,b,], Xing Xiaolei[a,b], Ren Xuejun[c], Yang Qingxiang[a],

a State Key Laboratory of Metastable Materials Science & Technology, Yanshan University, Qinhuangdao 066004, PR China

b College of Mechanical Engineering, Yanshan University, Qinhuangdao 066004, PR China

c School of Engineering, Liverpool John Moores University, Liverpool L3 3AF, UK

Abstract

Niobium carbide (NbC) reinforced metal matrix composite (MMC) coatings have been widely applied for surface strengthening, and the precipitation of granular primary NbC may be a feasible way to improve the wear resistance of coating. In this work, MgAl2O4 was selected to promote the precipitation of granular primary NbC, and a combination of experimental observations and first-principles modelling were carried out to investigate it. The calculation results show that, misfit between MgAl2O4 and NbC is 8.7%, which indicates that the MgAl2O4 nucleating effecting on NbC is structurally potent. In order to eliminate the interference combination between different elements, the MgAl2O4 (1 1 1)/NbC (1 1 1) interface overlaps were selected, and four different element matches are designed: O(Mg)Nb, Al(Mg)Nb, Al(Mg)C and Mg(O)C. From the interfacial adhesion work and interfacial energy, the stability order of the four models can be found: O(Mg)Nb > Al(Mg)C > Al(Mg) Nb > Mg(O)C. Moreover, mixture bonding of metal bonds, ionic bonds and covalent bonds are formed at the interface of O(Mg)Nb, Al(Mg)Nb, Al(Mg)C and Mg(O)C. From the experimental results, core-shell primary NbC carbides can be observed in M-1 (0.5 wt% AlMg alloy powder) coating and the core of carbide is identified to be MgAl2O4. Besides, the wear loss of M-1 coating is decreased, compared to M-0 coating.

1. Introduction

Niobium carbide (NbC) reinforced Fe-based composite coatings have been widely applied for surface strengthening of iron-based materials due to their high hardness, excellent wear resistance and price advantage [1,2]. It is generally believed that the main factors affecting the wear resistance of carbide-reinforced composite coatings are the hardness, size, distribution and morphology of carbides [3,4]. In order to meet the ever-increasing demand for harsh working conditions, it is necessary to find some ideas to further improve the wear resistance of the coating. Among these factors, morphology of carbide is an interesting but noteworthy factor. The niobium carbide can precipitate in form of granular primary and flaky eutectic ones based on the precipitation order of NbC and Fe matrix. For wear-resistant coatings, granular carbides are superior to other shapes of carbides [5,6]. Therefore, it is a feasible way to promote the precipitation of granular niobium carbide to improve the wear resistance of the coating. Magnesium aluminum spinel (MgAl2O4) has been widely used as substrates for the growth of thin films because of its structural, chemical stability and low thermal expansion coefficient [7–9]. Parker et al. [10] added MgAl2O4 as a nucleation core into acicular ferritic steel to promote the precipitation of TiN, thereby controlling the heat affected zone during the welding

process. They found that $MgAl_2O_4$ can be used as the nucleation core of TiN, and they have the same crystal orientation. NbC has the same MC type crystal structure as TiN. Therefore, if it has a good interfacial bonding properties between NbC and $MgAl_2O_4$, the $MgAl_2O_4$ could be used tentatively as the nucleation core of NbC to promote the precipitation of granular primary NbC. In order to understand the nuclei effect $MgAl_2O_4$ on NbC carbide, the interfacial properties of NbC/$MgAl_2O_4$ interface should be investigated. However, it is difficult to research NbC/$MgAl_2O_4$ interface by experiment. First principles calculation is an effective method to study the interface of materials. Li et al. [11] studied the surface relaxation, surface energies, surface grand potentials and electronic properties of different terminations of $MgAl_2O_4$ (1 1 1) surfaces and found that, Mg(Al)-termination is the most stable in O- and Al-rich environments. Lv et al. [12] investigated the nature of fluorine adsorption on pure and N doped $MgAl_2O_4$ surface and found that nitrogen doped $MgAl_2O_4$ is a promising candidate for fluorine removal. Yang et al. [13] researched the electronic property and bonding configuration of NbC (1 1 1)/NbN (1 1 1) interface and indicated that interface termination structure plays an important role on influencing the interfacial stability.

In this work, the mechanical parameters (elastic modulus, bulk modulus and shear modulus) of $MgAl_2O_4$ and NbC, and the misfit between $MgAl_2O_4$ and NbC were studied. The interfacial atomic structure, interfacial work of adhesion, interfacial energy and charge distribution of NbC (1 1 1)/$MgAl_2O_4$ (1 1 1) interfaces were calculated. Meanwhile, the microstructure of core-shell carbide in coatings were investigated. Subsequently, the hardness and wear resistance of the coatings were analyzed.

2. Experimental methods and computational details

2.1. Experimental methods

The Fe matrix NbC composites coatings were prepared by gas metal arc welding (GMAW) hardfacing technology. The flux-cored wires were deposited on Q235 low-carbon steel plates. The core of flux-cored wire was made of graphite, ferrochromium, ferrovanadium, ferromanganese, ferrosilicon and ferroniobium powder, and it was covered by low carbon steel strip of H08A. The details of flux-cored wire manufacturing and hardfacing process were based on our previous work [14]. The compositions of the coatings with and without AlMg (50%Al and 50% Mg) powder are listed in Table 1. The phase identification of the coatings were carried out on a Rigaku D/Max-2500/PC X-ray diffraction (XRD) with CuKa operating at 40 kV. The hardfacing specimens were etched with 4% nitric acid alcohol. The microstructure characterization of coatings was performed with a HITACHI S-4800 scanning electron microscope (FE-SEM) and a JEM-2100 transmission electron microscopy (TEM) equipped with an energy-dispersive spectroscopy (EDS).

Wear resistance test was evaluated by abrasive belt type wear testing machine in dry friction and SiC of 40 mesh was used as the abrasive material. The specimen size, loading force and wear velocity were 20mm×10mm×15 mm, 100 g and 1.8×104 mm/min, respectively. The wear loss values were obtained by the averages of six measurements. The hardness was measured using a HR-105A Rockwell hardness tester and the value was obtained by the averages of ten measurements.

2.2. Computational details

First-principles calculations based on density functional theory (DFT) with ultrasoft pseudopotentials were employed to evaluate some mechanical properties of NbC and MgAl2O4, and bond structures of NbC (1 1 1)/MgAl2O4 (1 1 1) interface. The calculations were performed by using Cambridge Sequential Total Energy Package (CASTEP) [15]. The exchange-correlation energy was evaluated by generalized gradient approximation (GGA) with Perdew-Burke-Ernzerhof (PBE) functional [16]. The mechanical parameters of NbC and MgAl2O4 were calculated through the Voigt-Reuss-Hill (VRH) approximation method [17]. On the basis of convergence tests, plane–wave cutoff energy was set at 540 eV and Brillouin zone sampling was set at 16×16×16 Monkhorst-Pack mesh for bulk calculation and 8×8×1 Monkhorst-Pack mesh for interface calculation. In order to eliminate the long interactions from periodic boundary condition calculation, a 12 Å vacuum space along the c-axis was used during interface calculation. For the convergence tolerances, the energy, the maximum force and maximum displacement were set as 1×10−5 eV/atom, 0.01 eV/Å and 1×10−3 Å, respectively.

3. Bulk and interface properties

3.1. Bulk properties of MgAl2O4 and NbC

The structures of MgAl2O4 and NbC are shown in Fig. 1. The MgAl2O4 crystal is a cubic spinel one with space group Fd-3m, No. 227 [18]. In the crystal structure, O atoms are arranged in a cubic packing, within the unit cell; Mg atoms partly occupy tetrahedral interstices between O atoms, and the smaller Al atoms are partly sited in octahedral interstices. Some previous investigations [19] indicate that, carbon poor niobium carbide may form at elevated temperature. And our previous work [20] shows that, the chemical stoichiometry of niobium carbide in the coating is very close to NbC. Therefore, NbC was used as niobium carbide model to do calculation. The NbC crystal belongs to group Fm-3m, No. 225 [21]. Before the interface calculations, the bulk models of MgAl2O4 and NbC were calculated and the results were compared with other experimental and calculated values to examine the reliability of the model [11,18,22–25]. The bulk (B) and shear (G) modulus can be obtained directly from elastic constant calculation based on VRH approximation. The poisson's ratio (ν) and elastic modulus (E) could be get from B and G by the following equations:

$$E = 9BG/(3B + G) \quad (1)$$

$$\nu = (3B - 2G)/2(3B + G) \quad (2)$$

The calculated results are shown in Table 2. The calculated lattice parameters of NbC and MgAl2O4 are 4.469 Å and 8.192 Å, respectively.

Lattice mismatch is a very important parameter for the investigation of heterogeneous nucleation system [26]. The lattice mismatch between them was estimated by the equation:

$$\delta = 2 \times \left(2\alpha_{NbC} - \alpha_{MgAl_2O_4}\right)/\left(2\alpha_{NbC} + \alpha_{MgAl_2O_4}\right) \quad (3)$$

where α is the lattice parameter of NbC or MgAl2O4.
After calculation from Eq. (3), the lattice mismatch between NbC and MgAl2O4 is 8.7%. The AlMg alloy power will be oxidized into MgAl2O4 or a mixture of MgO and Al2O3 during

welding process [9,27,28]. The formation energy of MgAl2O4 from MgO and Al2O3 can be obtained by follows:

$$E^{for}_{MgAl_2O_4} = E^{bulk}_{MgAl_2O_4} - E^{bulk}_{MgO} - E^{bulk}_{Al_2O_3} \quad (4)$$

The formation energy of MgAl2O4 is −0.21 eV, which proves that MgAl2O4 is more stable than MgO and Al2O3 mixture. Therefore, MgAl2O4 can be obtained from oxidation of AlMg alloy powder.

3.2. Interface model and adhesion work between NbC and MgAl2O4

The lattice mismatch of NbC and MgAl2O4 is 8.7%, which is less than 12%. It indicates that the MgAl2O4 nucleating agent effecting on NbC is structurally potent [26]. Therefore, the atomic bonding between MgAl2O4 and NbC interfaces need to be studied to learn the combination between them. In order to eliminate the interference combination between different elements, the MgAl2O4 (1 1 1)/NbC (1 1 1) interface overlaps were selected, and six different element matches are designed: Mg-Nb, Mg-C, Al-Nb, Al-C, O-Nb and O-C. There are eight different surface terminations in MgAl2O4 (1 1 1) surface, and the order of their surface energy is as follows [11]: Mg(O) < Al (Mg) < O(Mg) < O (Al) < O2(Al) < Mg(Al) < O2(Mg) < Al(O). The surface energy of Mg(O), Al(Mg) and O(Mg) terminate surfaces is the lowest among Mg, Al and O terminate ones, which indicates that they are more stable and difficult to cohere with other compounds. Therefore, the most stable Mg (O), Al(Mg) and O(Mg) termination surfaces were selected to combine with NbC (1 1 1) surfaces. The numbers of Nb and C termination layers are 13 [13] and the Mg(O), Al(Mg) and O(Mg) termination layers are 11, 13 and 17 [11]. During the calculation, it is found that the geometric optimizations of the O(Mg)C and Mg(O)Nb models do not converge, so only the O(Mg)Nb, Al(Mg)Nb, Al(Mg)C and Mg(O)C models were calculated further. The interface calculation models are shown in Fig. 2.

During the calculation, the interface distance d0 (Å) of four models before relaxation were set based on the atomic distances of NbO, NbAl, AlC and MgC compounds, respectively. The interface distance after full relaxation is defined as d1(Å). The adhesion work can reflect the binding strength of the material interfaces. The interface adhesion work (*Wad*) equation is shown as follows [29,30]:

$$W_{ad} = \left(E_{MgAl_2O_4} + E_{NbC} - E_{MgAl_2O_4/NbC}\right)/A \quad (5)$$

where *EMgAl2O4*and *ENbC* denote the total energies of MgAl2O4 and NbC relaxed; *EMgAl2O4*/*NbC* denotes the total energy of the interface system; *A* is the interface area. The interfacial energy (*γ*int) can be get from the following equation [31,32]:

$$\gamma_{\text{int}} = \sigma_{MgAl_2O_4} + \sigma_{NbC} - W_{ad} \quad (6)$$

where *σMgAl2O4* and *σNbC* are the surface energy of MgAl2O4 and NbC relaxed [11,13]; *Wad* is the adhesion work of MgAl2O4 (1 1 1)/NbC (1 1 1) interfaces.

The calculation results of the interfaces are shown in Table 3. It can be seen that the *Wad* of O(Mg)Nb, Al(Mg)Nb, and Al(Mg)C are positive, which indicates that separating the interface into two free surfaces is energy needed. And that of O(Mg)Nb is the largest, which indicates that the interface is the most stable. It is noteworthy that the*Wad* of Mg(O)C interface is a negative, which means that the Mg(O)C interface is unstable. From the *Wad*, the stability order

of four models is as following: O(Mg)Nb > Al(Mg)C > Al(Mg)Nb > Mg(O)C. The γint can also reflect the stability of interface. The lower the γint is, the more stable the interface structure is. From the γint, the stability order of the four models can be found: O(Mg)Nb > Al(Mg)C > Al(Mg)Nb > Mg(O)C. d0 and d1 are also shown in Table 3. It can be seen that the interface distance of four models are substantially the same with the atom distance of NbO, NbAl, AlC and MgC compounds.

3.3. Bonding structures of interfaces

The combination of interfaces are closely related to its bonding structures. The partial electronic density of states (PDOS) of the interfaces are shown in Fig. 3. It can be seen clearly that the N(EF) of all the interface models are larger than 0, which indicates that the four interfaces present the metallic characteristic. Besides, the orbits overlapped can be seen at the O-Nb, Al-Nb, Al-C and Mg-C interfaces, which illustrates the formation of covalent bonds by the orbits hybridization.

To further clarify the spatial distribution of electrons and the relative electron transfer of four interfaces, the charge densities and charge density differences of the interface system were calculated. The charge density can be available directly and the charge density difference $\Delta\rho MgAl2O4/NbC$ can be get as follows [33,34]:

$$\Delta\rho_{MgAl_2O_4/NbC} = \rho_{Total} - \rho_{MgAl_2O_4} - \rho_{NbC} \quad (7)$$

where, $\rho Total$ is the total charge density of the MgAl2O4/NbC interface systems; $\rho MgAl2O4$and ρNbC are the charge densities for the MgAl2O4 and NbC relaxed isolated slabs, respectively. The plots of charge densities and charge density differences along plane (110_), which pass through the interface atoms, are shown in Fig. 4. From Fig. 4(a), the directional spatial distribution of electrons can be seen at the interfaces, which indicates the formation of covalent bonds. The calculated bond populations are listed in Table 4. From it, the bond populations of O(Mg)Nb, Al(Mg)C and Al(Mg)Nb interfaces are positive, which means the formation of strong covalent bonds.

However, that of Mg(O)C interface is negative, which means the formation of unstable antibond. They are consistent with the adhesion work and interfacial energy results. From Fig. 4(b), charge depleted and acquired region can be observed clearly at the interfaces, which presents the ionic properties of the interfaces. The detail of charge transfer can be analyzed by the atoms charges of the interface models listed in Table 5. Compared to MgAl2O4 or NbC layers, the charges of atoms at the interface are changed, which indicates the charges transfer between O-Nb, Al-Nb, Al-C and Mg-C interface atoms. In general, mixture bonding of metal bonds, ionic bonds and covalent bonds are formed at the interface of O(Mg)Nb, Al(Mg)Nb, Al(Mg)C and Mg(O)C modes. Although the actual interface situation is much more complex, the O-Nb, Al-Nb, Al-C and Mg-C atom connection may play an active role in the combination of MgAl2O4 and NbC.

4. Morphology of carbides and wear resistance of coatings

4.1. Core shell carbide in coatings

Fig. 5 is the XRD diffraction pattern of M-0 and M-1 coatings. It can be seen that the diffraction peaks of the two coatings are basically the same, which are composed of MC type carbide, α

phase and γ phase. None of MgAl2O4 diffraction peaks can be observed. The microstructures of two coatings are shown in Fig. 6. It can be seen that the NbC carbides in M-0 coating are mainly precipitated in form of eutectic carbide. In the M-1 coating, except for eutectic carbide, primary NbC carbides can also be observed. Besides, core-shell structure can be found in some primary NbC carbides. To identify the core of carbides, its TEM morphology, selected area electron diffraction (SAED) pattern and EDS element analysis were obtained, which are shown in Fig. 7(a) and (b). From Fig. 7(a), the core shell structure is also observed. As can be seen in Fig. 7(b) the core area is of face centered cubic structure with a zone axis [1 1 2], and the lattice parameter is about 8.17 Å, which is matched well with the other experimental lattice parameter of MgAl2O4 (8.09 Å) [35]. The EDS analysis results are listed in Table 6. The core area are mainly composed of Mg, Al and O elements, and very little Fe element can be found. The atomic ratios of Mg, Al and O are very close to 1:2:4. Therefore, the core of the core-shell carbide is considered as MgAl2O4.

4.2. Hardness and wear resistance of coatings

The hardness and wear loss of the M-0 and M-1 coatings are shown in Fig. 8. The hardness of M-1coating is slightly higher than that of M-0 coating. However, the wear loss of M-1 is 0.53 g/N cm2, significantly lower than that of M-0 coating, which indicates that promoting the precipitation of primary carbide is an effective method to improve wear resistance of coatings. To achieve a better understand of the wear loss results, the worn surfaces morphologies of two coatings are shown in Fig. 9. From Fig. 9(a), very deep furrows appear in the M-0 coating. The high strain energy and negative interfacial energy of NbC and Fe interface model has been reported [25], which may indicate that the combination between NbC and Fe matrix is not so good. So, during the wear process, eutectic carbide will loosen or even slide on the Fe matrix, and this may be the source of the deep furrows. From Fig. 9(b), broken primary NbC carbides can be observed in M-1 coating, and the broken carbides are considered as reinforcements to block the abrasion paths [3,36,37], which is beneficial to decrease the wear loss of the coating.

5. Conclusion

(1) The mismatch between MgAl2O4 and NbC is 8.7%, which is less than 12%. It indicates that MgAl2O4 nucleating agent effecting on NbC is structurally potent.
(2) From the interfacial adhesion work and interfacial energy, the stability order of the four models can be gotten: O(Mg)Nb > Al (Mg)C > Al(Mg)Nb > Mg(O)C. There are mixture bonding structures of O-Nb, Al-Nb, Al-C and Mg-C between MgAl2O4 and NbC.
(3) Core shell primary NbC carbides can be observed in M-1 coating and the core of carbide is considered to be MgAl2O4 based on identification.
(4) The wear loss of M-1 coating is 0.53 g/N cm2, which is less than that of M-0 coating. It means that the wear resistance of M-1 coating is improved.

Acknowledgement

The authors would like to express their gratitude for projects supported by the National Natural Science Foundation of China, China (No.51471148, No. 51771167 and No. 51705447), the Hebei province Basic Research Foundation of China, China (No. 16961008D).

References

[1] X.H. Wang, Z.D. Zou, S.Y. Qu, S.L. Song, Microstructure and wear properties of Fe based hardfacing coating reinforced by TiC particles, J. Mater. Process. Technol.168 (2005) 89–94.

[2] R. Colaço, R. Vilar, Laser rapid-alloy prototyping for the development of wear resistant Fe–Cr–C/NbC composite materials, J. Laser Appl. 15 (2003) 267–272.
[3] L. Zhong, F. Ye, Y. Xu, J. Li, Microstructure and abrasive wear characteristics of in situ vanadium carbide particulate-reinforced iron matrix composites, Mater. Des. 54 (2014) 564–569.
[4] S. Wei, J. Zhu, L. Xu, L. Rui, Effects of carbon on microstructures and properties of high vanadium high-speed steel, Mater. Des. 27 (2006) 58–63.
[5] H. Cao, X. Dong, S. Chen, M. Dutka, Y. Pei, Microstructure evolutions of graded high-vanadium tool steel composite coating in-situ fabricated via atmospheric plasma beam alloying, J. Alloy. Compd. 720 (2017) 169–181.
[6] J.W. Park, C.L. Huo, S. Lee, Composition, microstructure, hardness, and wear properties of high-speed steel rolls, Metall. Mater. Trans. A 30 (1999) 399–409.
[7] G. Fiquet, P. Richet, G. Montagnac, High-temperature thermal expansion of lime, periclase, corundum and spinel, Phys. Chem. Miner. 27 (1999) 103–111.
[8] S. Köstlmeier, C. Elsässer, B. Meyer, M.W. Finnis, A density functional study of interactions at the metal–ceramic interfaces Al/MgAl2O4 and Ag/MgAl2O4, Phys. Status Solidi 166 (1998) 417–428.
[9] M. Catti, G. Valerio, R. Dovesi, M. Causà, Quantum-mechanical calculations of the solid-state equilibrium MgO + alpha-Al2O3 + MgAl2O4 (spinel) versus pressure, Phys. Rev. B 49 (1994) 1316764–11314187.
[10] J.S. Park, D.H. Kim, J.H. Park, TEM characterization of a TiN-MgAl2O4 epitaxial interface, J. Alloy. Compd. 695 (2017) 476–481.
[11] X. Li, Q. Hui, D.Y. Shao, J.J. Chen, C.M. Li, N.P. Cheng, Stability and electronic structure of MgAl2O4 (111) surfaces: a first-principles study, Comput. Mater. Sci.112 (2016) 8–17.
[12] X. Lv, Z. Xu, J. Li, J. Chen, Q. Liu, Investigation of fluorine adsorption on nitrogen doped MgAl2O4 surface by first-principles, Appl. Surf. Sci. 376 (2016) 97–104.
[13] J. Yang, J. Huang, D. Fan, S. Chen, First-principles investigation on the electronic property and bonding configuration of NbC (111)/NbN (111) interface, J. Alloy. Compd. 689 (2016) 874–884.
[14] X. Yun, Y.F. Zhou, B. Zhao, X.L. Xing, J. Yang, Y.L. Yang, Q.X. Yang, Influence of nano-Y2O3 on wear resistance of hypereutectic Fe–Cr–C hardfacing coating, Tribol. Lett. 58 (2015) 23.
[15] D. Vanderbilt, Soft self-consistent pseudopotentials in a generalized eigenvalue formalism, Phys. Rev. B 41 (1990) 7892–7895.
[16] J.P. Perdew, E.R. McMullen, A. Zunger, Density-functional theory of the correlation energy in atoms and ions: a simple analytic model and a challenge, Phys. Rev. A 23(1981) 2785–2789.
[17] W. Boas, Physical properties of crystals, their representation by tensors and matrices,J. Mech. Phys. Solids 6 (1958) 328–329.
[18] T.V. Dunaitseva, L.B. Romanovskii, E.G. Potap, Y.I. Savchenko, V.A. Perepelitsyn,N.F. Seliverstov, G.G. Galimov, Sintering of synthesized magnesia spinels and the systems based on them, Refractories 31 (1990) 615–618.
[19] G.K. Tirumalasetty, M.A. van Huis, C.M. Fang, Q. Xu, F.D. Tichelaar, D.N. Hanlon, J. Sietsma, H.W. Zandbergen, Characterization of NbC and (Nb, Ti)N nanoprecipitates in TRIP assisted multiphase steels, Acta Mater. 59 (2011) 7406–7415.
[20] C. Zhao, Y. Zhou, X. Xing, S. Liu, X. Ren, Q. Yang, Investigation on the relationship between NbC and wear-resistance of Fe matrix composite coatings with different C contents, Appl. Surf. Sci. 439 (2018) 468–474.

[21] Y.S. Karimov, T.G. Utkina, Superconductivity of nonstoichiometric niobium carbide, Jetp Lett. 51 (1990) 528.
[22] A. Teresiak, H. Kubsch, X-ray investigations of high energy ball milled transition metal carbides, Nanostructured Materials 6 (1995) 671–674.
[23] A.M. Nartowski, I.P. Parkin, M. Mackenzie, A.J. Craven, Solid state metathesis:synthesis of metal carbides from metal oxides, J. Mater. Chem. 11 (2001) 3116–3119.
[24] L. Wu, Y. Wang, Z. Yan, J. Zhang, F. Xiao, B. Liao, The phase stability and mechanical properties of Nb–C system: Using first-principles calculations and nanoindentation, J. Alloy. Compd. 561 (2013) 220–227.
[25] J.H. Jang, C.H. Lee, Y.U. Heo, D.W. Suh, Stability of (Ti, M)C (M=Nb, V, Mo and W) carbide in steels using first-principles calculations, Acta Mater. 60 (2012) 208–217.
[26] B.L. Bramfitt, The effect of carbide and nitride additions on the heterogeneous nucleation behavior of liquid iron, Metall. Trans. 1 (1970) 1987–1995.
[27] J.S. Park, C. Lee, J.H. Park, Effect of complex inclusion particles on the solidification structure of Fe-Ni-Mn-Mo Alloy, Metall. Mater. Trans. B 43 (2012) 1550–1564.
[28] H. Sukegawa, Y. Miura, S. Muramoto, S. Mitani, T. Niizeki, T. Ohkubo, K. Abe, M. Shirai, K. Inomata, K. Hono, Enhanced tunnel magnetoresistance in a spinel oxide barrier with cation-site disorder, Phys. Rev. B 86 (2012) 184401.
[29] L.M. Liu, S.Q. Wang, H.Q. Ye, First-principles study of polar Al/TiN (111) interfaces, Acta Mater. 52 (2004) 3681–3688.
[30] T.D. Kuhne, T.A. Pascal, E. Kaxiras, Y. Jung, New insights into the structure of the vapor/water interface from large-scale first-principles simulations, J. Phys. Chem. Lett. 2 (2011) 105–113.
[31] X. Torrelles, F. Wendler, O. Bikondoa, H. Isern, W. Moritz, G.R. Castro, Structure of the clean NiAl (110) surface and the Al2O3/NiAl (110) interface by measurements of crystal truncation rods, Surf. Sci. 487 (2001) 97–106.
[32] W. Liu, J.C. Li, W.T. Zheng, Q. Jiang, NiAl (110)/Cr (110) interface: A density functional theory study, Phys. Rev. B 73 (2006) 205421.
[33] W. Kohn, L.J. Sham, Quantum density oscillations in an inhomogeneous electron gas, Phys. Rev. 137 (1965) 1697–1705.
[34] A. Arya, E.A. Carter, Erratum: structure, bonding, and adhesion at the TiC (100)/Fe (110) interface from first principles, J. Chem. Phys. 120 (2004) 1142.
[35] S. Köstlmeier, C. Elsässer, B. Meyer, M.W. Finnis, A density functional study of interactions at the metal-ceramic interfaces Al/MgAl2O4 and Ag/MgAl2O4, Phys.Status Solidi 166 (1998) 417–428.
[36] T. Gong, P. Yao, X. Zuo, Z. Zhang, Y. Xiao, L. Zhao, H. Zhou, M. Deng, Q. Wang, A. Zhong, Influence of WC carbide particle size on the microstructure and abrasive wear behavior of WC–10Co–4Cr coatings for aircraft landing gear, Wear 362–363 (2016) 135–145.
[37] L. Zhong, Y. Xu, F. Ye, In situ NbC particulate-reinforced iron matrix composite:microstructure and abrasive wear characteristics, Tribol. Lett. 47 (2012) 253–259.

Table 1
Compositions of coatings (wt.%).

No.	C	Nb	Cr	Mn	Si	V	Mg-Al	Fe
M-0	1.15	4.48	5.43	1.20	1.35	0.51	–	Bal.
M-1	1.10	4.45	5.32	1.31	1.29	0.47	0.50	Bal.

Table 2
Calculated results of lattice constant, elastic modulus, bulk modulus, shear modulus and passion ratio.

Phase	Lattice constants a(Å)	Elastic modulus E (GPa)	Bulk modulus B (GPa)	Shear modulus G (GPa)	Passion ratio ν
NbC	4.469 4.468 [20], 4.47 [21]	509 486 [22]	316 318 [23]	205 198 [22]	0.23 0.22 [22]
$MgAl_2O_4$	8.192 8.195 [11], 8.155 [18]	249	175 173 [11]	99	0.26

Table 3
Adhesion work (J/m^2), interface energy (J/m^2) and interface distance (Å).

Interface	O(Mg)Nb	Al(Mg)Nb	Al(Mg)C	Mg(O)C
W_{ad} (J/m^2)	3.28	0.81	1.63	−0.28
γ_{int} (J/m^2)	4.31	5.01	4.32	6.17
d_1 (Å)	1.98	2.69	1.96	2.28
d_0 (Å)	2.10 (NbO)	2.89 (NbAl)	1.93 (AlC)	2.21 (MgC)

Table 4
Calculated Mulliken overlap population (MOP): Bond population.

Interface	O(Mg)Nb (O-Nb)	Al(Mg)Nb (Al-Nb)	Al(Mg)C (Al-C)	Mg(O)C (Mg-C)
Bond populations	0.99	0.62	0.76	−0.58

Table 5
Calculated Mulliken overlap population (MOP): Atom charges (e).

Layer	O(Mg)Nb		Al(Mg)Nb		Al(Mg)C		Mg(O)C	
	Atom	Charges	Atom	Charges	Atom	Charges	Atom	Charges
$MgAl_2O_4$ layer	O	−1.10	Mg	1.55	Mg	1.55	Al	1.50
	Al	1.43	O	−1.10	O	−1.10	Mg	1.56
	O	−1.09	O	−1.10	O	−1.09	O	−1.11
	O	−1.07	Al	1.42	Al	1.43	O	−1.10
	Mg	1.55	O	−1.14	O	−1.13	Al	1.48
	Al	1.37	O	−1.07	O	−1.07	O	−1.07
	Mg	1.72	Mg	1.56	Mg	1.55	O	−0.90
Interface	O	−0.89	Al	1.01	Al	1.45	Mg	1.67
	Nb	0.35	Nb	−0.14	C	−0.87	C	−0.75
NbC layer	C	−0.69	C	−0.70	Nb	0.70	Nb	0.73
	Nb	0.79	Nb	0.79	C	−0.71	C	−0.71
	C	−0.72	C	−0.73	Nb	0.74	Nb	0.72
	Nb	0.73	Nb	0.73	C	−0.71	C	−0.71
	C	−0.72	C	−0.71	Nb	0.72	Nb	0.72
	Nb	0.73	Nb	0.71	C	−0.71	C	−0.72
	C	−0.72	C	−0.71	Nb	0.70	Nb	0.71
	Nb	0.72	Nb	0.71	C	−0.71	C	−0.71

Table 6
EDS analysis results of core area.

Chemical element	Weight percentage	ATOM percentage
O	42.13	54.66
Mg	16.71	14.27
Al	39.68	30.52
Fe	1.48	0.55

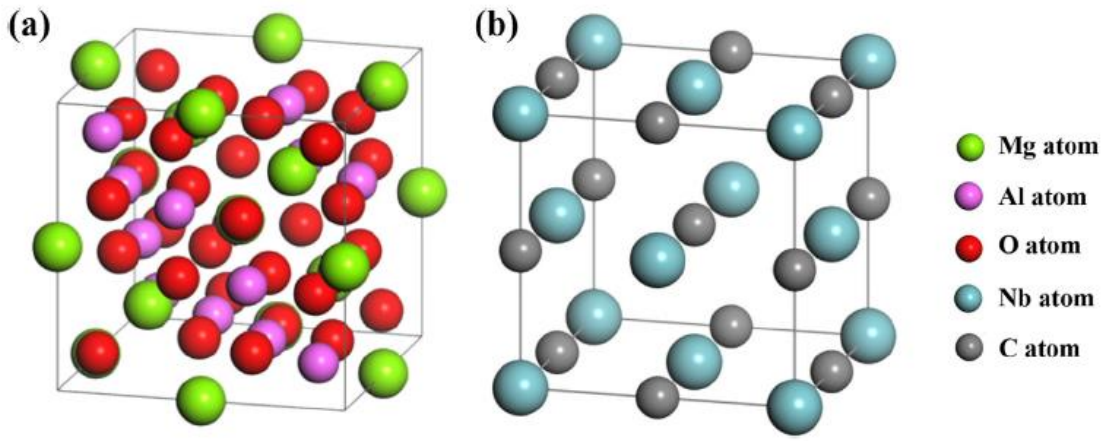

Fig. 1. Crystal structures of (a) $MgAl_2O_4$ and (b) NbC.

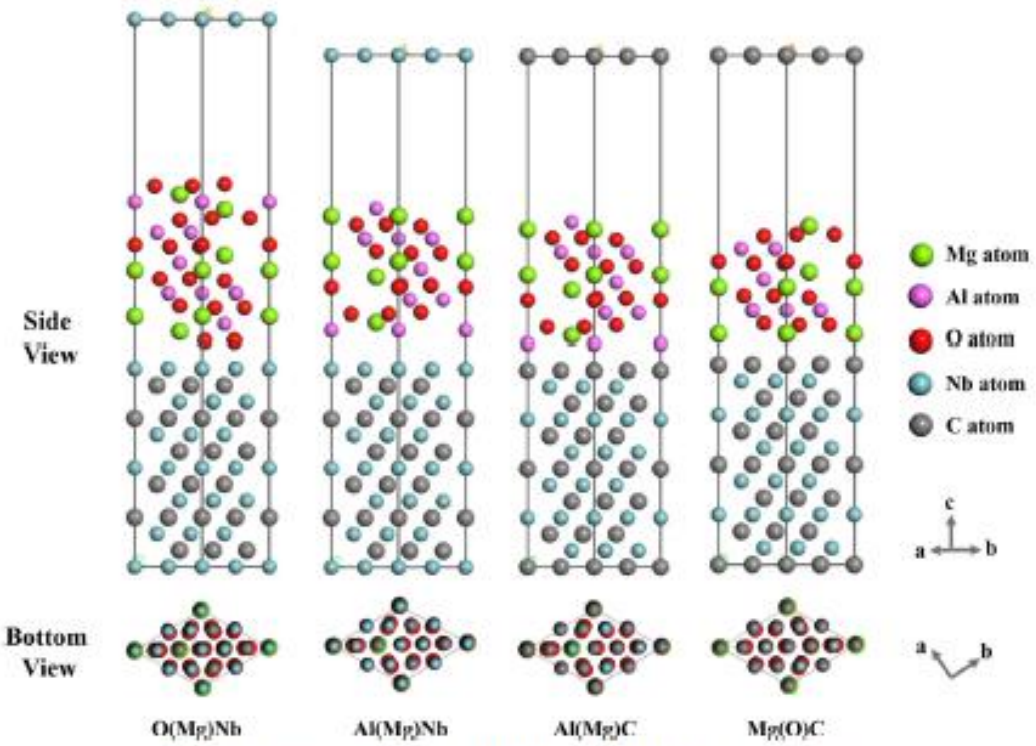

Fig. 2. Interface models of $MgAl_2O_4$ (1 1 1)/NbC (1 1 1) interface overlaps.

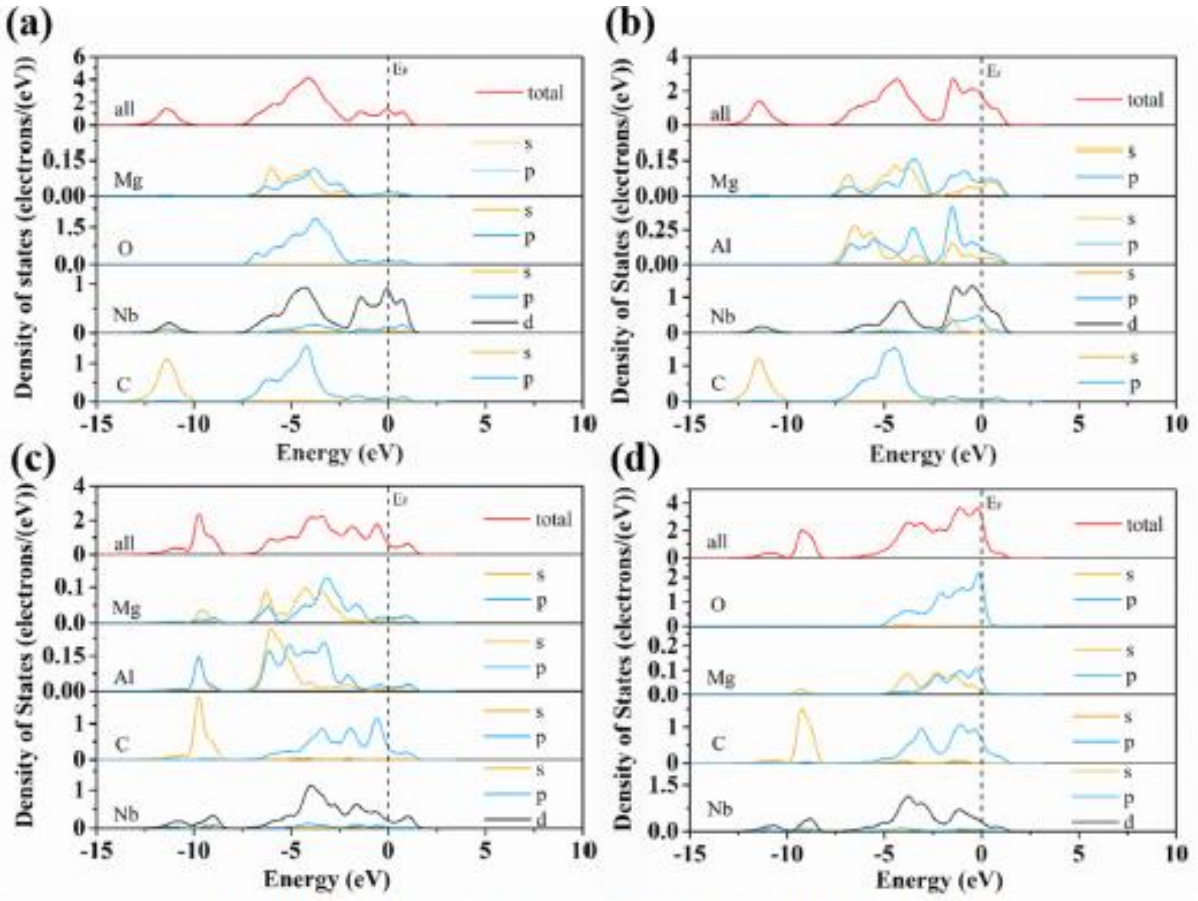

Fig. 3. PDOS of the interface models: (a) O(Mg)Nb, (b) Al(Mg)Nb, (c) Al(Mg)C, (d) Mg(O)C.

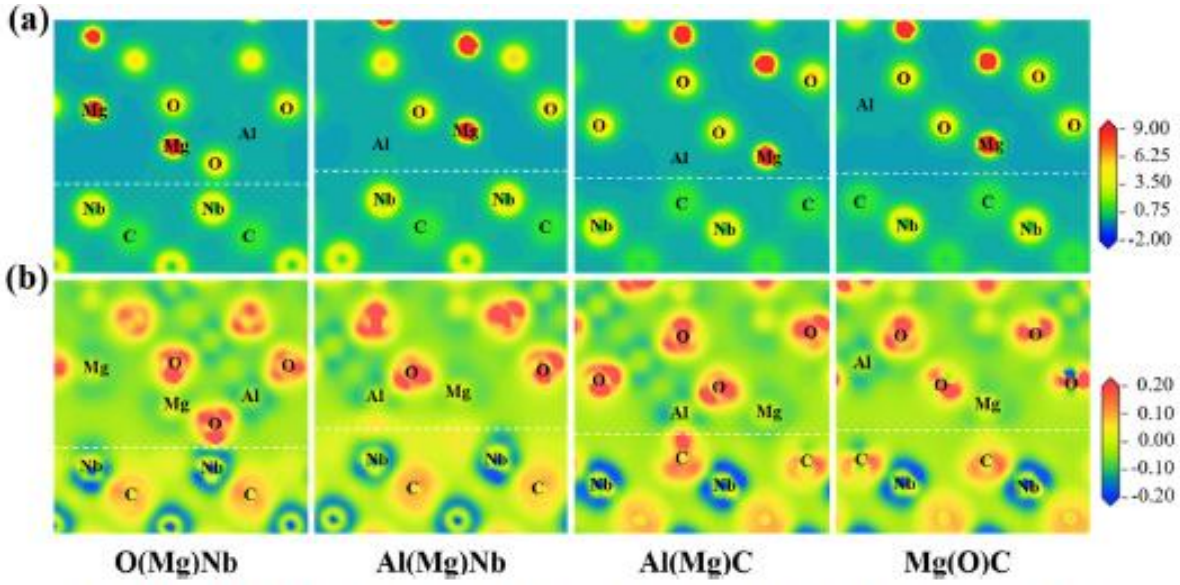

Fig. 4. Charge density and charge density difference of interface models: (a) Charge density and (b) charge density difference.

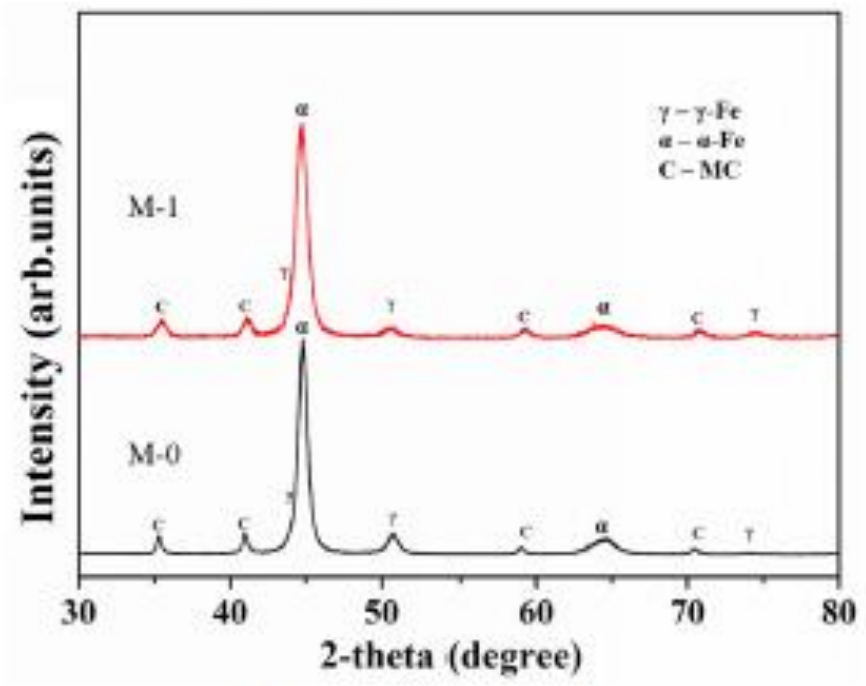

Fig. 5. XRD results of two coatings.

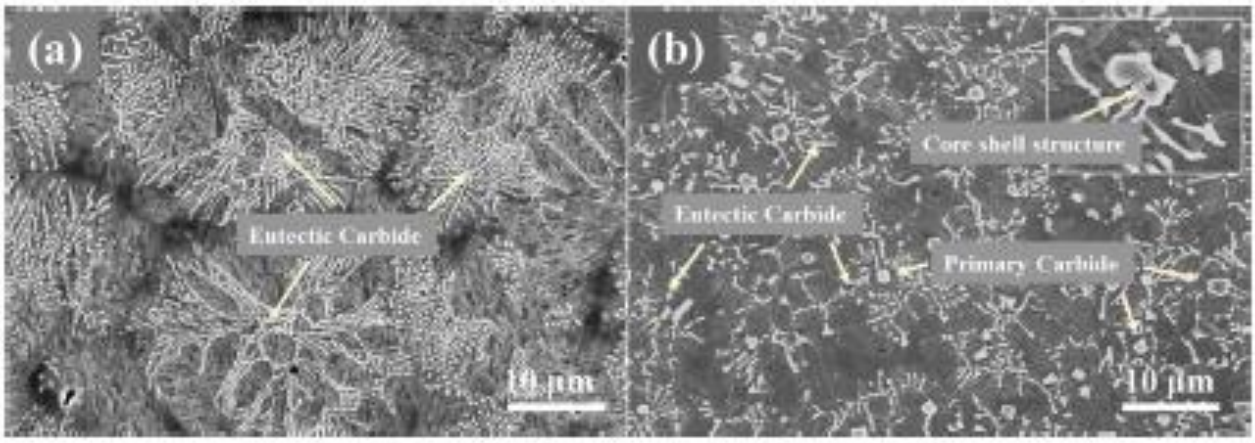

Fig. 6. Morphologies of the coatings. (a) M-0 and (b) M-1.

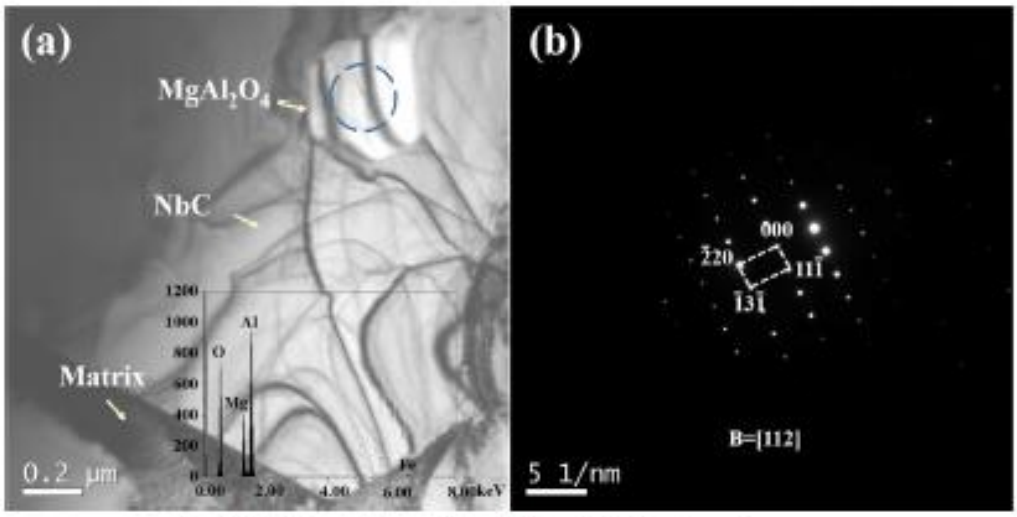

Fig. 7. TEM image of core shell carbide and SEAD pattern of core area.

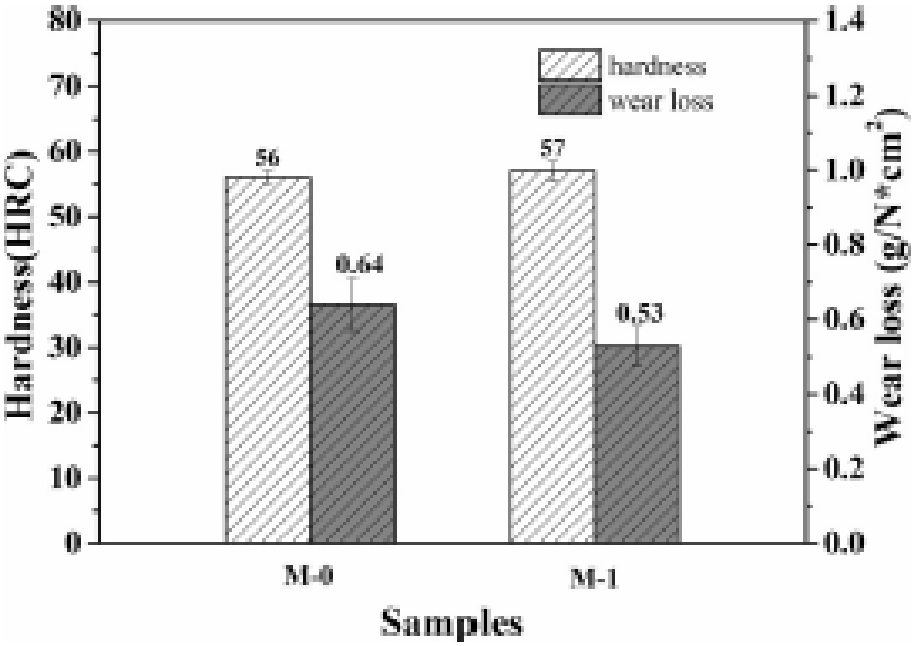

Fig. 8. Hardness and wear loss of two coatings.

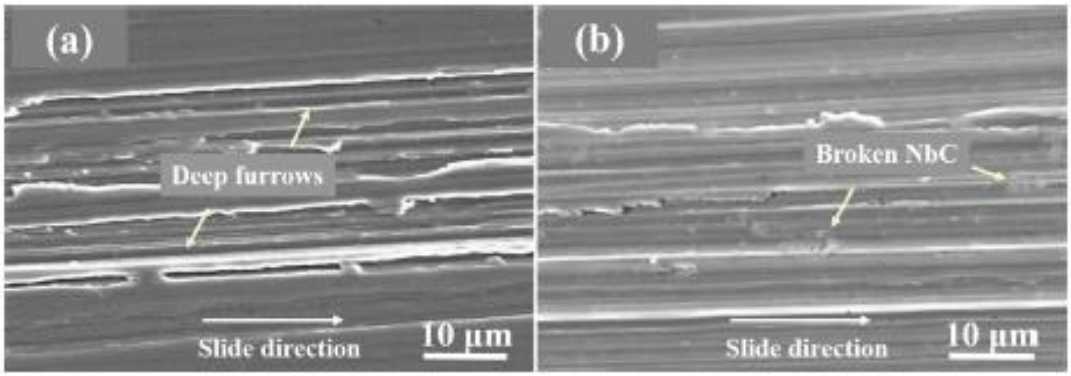

Fig. 9. Worn surfaces morphology of the two matings (a) M-0 and (b) M-1.